Structure, Electronic States, and Anion–Binding Properties of Cyclo[4]naphthobipyrroles

ARTICLE *in* THE JOURNAL OF PHYSICAL CHEMISTRY A · JANUARY 2014

Impact Factor: 2.69 · DOI: 10.1021/jp412139r · Source: PubMed

THE JOURNAL OF PHYSICAL CHEMISTRY A

Article

pubs.acs.org/JPCA

Structure, Electronic States, and Anion-Binding Properties of Cyclo[4]naphthobipyrroles

Patrycja Kowalska,[†] Sylwester Gawinkowski,[†] Tridib Sarma,[‡] Pradeepta K. Panda,[‡] and Jacek Waluk*[,†]

[†]Institute of Physical Chemistry, Polish Academy of Sciences, Warsaw 01-224, Poland

[‡]School of Chemistry, University of Hyderabad, Hyderabad 500046, India

ABSTRACT: Three octaalkyl-substituted cyclo[4]-naphthobipyrroles, studied in solution in the form of their sulfates, reveal absorption and magnetic circular dichroism (MCD) spectra very similar to those of the parent cyclo[8]-pyrrole. A unique feature of these systems is a strong absorption in the near IR region. The analysis of MCD patterns based on a perimeter model reveals a hard-chromophore character of cyclo[4]naphthobipyrroles, i.e., ΔHOMO ≪ ΔLUMO. Comparison of Raman spectra obtained for crystalline samples and solutions, combined with the analysis of absorption and MCD spectra based on quantum chemical calculations reveals that cyclo[4]naphthobipyrroles exist in solutions as undissociated sulfates of the doubly protonated forms.

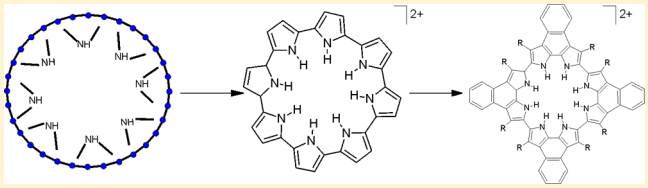

1. INTRODUCTION

Macrocyclic pyrrole derivatives that consist of more than four pyrrole rings or possess more than four bridging −CH═ units belong to the so-called expanded porphyrins, molecules with an inner cavity larger than in the parent compounds. Among them, aromatic expanded porphyrins are unique, owing to a larger number of π-electrons forming the aromatic cycle. These compounds have gained much attention due to interesting spectral, photophysical, structural, and complexing properties.[1−27] The latter include the ability to bind cations, anions, and neutral molecules, which makes expanded porphyrins good candidates for molecular receptors.[2,6,8,18,25,26] Regarding electronic transitions, these compounds often exhibit electronic absorption shifted to the red compared with porphyrins, sometimes very significantly. The absorption intensities are stronger than in porphyrins and the relative intensities of transitions to low- and high-energy states (Q/L and Soret/B bands) often change dramatically. These characteristics lead to applications in such areas as photodynamic therapy,[28,29] magnetic resonance imaging,[30] and design of new materials and sensors.[2,7,31] Regarding fundamental research, studies of expanded porphyrins may contribute to the understanding of various aspects of aromaticity, e.g., Hückel vs Möbius type.[14,16,21,32,33]

An interesting subclass of aromatic expanded porphyrins is cyclo[n]pyrroles, compounds in which the pyrrole units are directly linked.[34−53] Their fully protonated forms may assume high symmetry; as a consequence, degenerate excited states possessing magnetic moments are possible. The value of the magnetic moment can be determined from the analysis of magnetic circular dichroism (MCD) spectrum. We have previously investigated the electronic structure of three cyclo[n]pyrroles, with n = 6−8 using MCD spectroscopy.[36] It was demonstrated that the magnetic moments of protonated, dicationic forms decrease in the order 6 > 7 > 8; i.e., smaller values are observed for larger π-electron conjugation paths. This rather counterintuitive result could be explained using a perimeter model.[54] Recently, it was observed that extension of the aromatic π-cloud of the porphyrinoids through β-bipyrrole fusion resulted in dramatic effects on the structure and photophysical properties, including their nonlinear optical properties and also their coordination ability.[55−57]

In this work, we investigate the geometrical and electronic structure of three cyclo[4]naphthobipyrroles (**1a**−**1c**, Scheme 1), derivatives of cyclo[8]pyrrole (**2**). Their synthesis and initial studies have been reported recently.[55−57] A unique spectral feature of **1a**−**1c**, attractive from the point of view of possible applications, is the strong electronic absorption in the near IR, considerably red-shifted compared to the absorption of **2**. Using electronic and MCD spectroscopy combined with quantum-chemical calculations, we assign the electronically excited states and discuss the structure and symmetry of the chromophore. In particular, we address problems concerning the planarity and structure of the doubly protonated dicationic species. We also describe attempts to obtain neutral species and analyze spectral changes accompanying deprotonation.

2. EXPERIMENTAL AND COMPUTATIONAL DETAILS

The synthesis and purification of cyclo[4]naphthobipyrroles have been described elsewhere.[55,56] Absorption spectra were measured using a Shimadzu UV 3100 spectrophotometer. MCD measurements were carried out on an OLIS DSM 17 CD spectropolarimeter equipped with a permanent magnet. The MCD instrument was calibrated using camphorsulfonic acid-*d*. The value of the magnetic field (1.06 T) was determined using aqueous $CoSO_4$ solution. Two R955 photomultipliers and a

Received: December 11, 2013
Revised: January 20, 2014
Published: January 22, 2014

Scheme 1

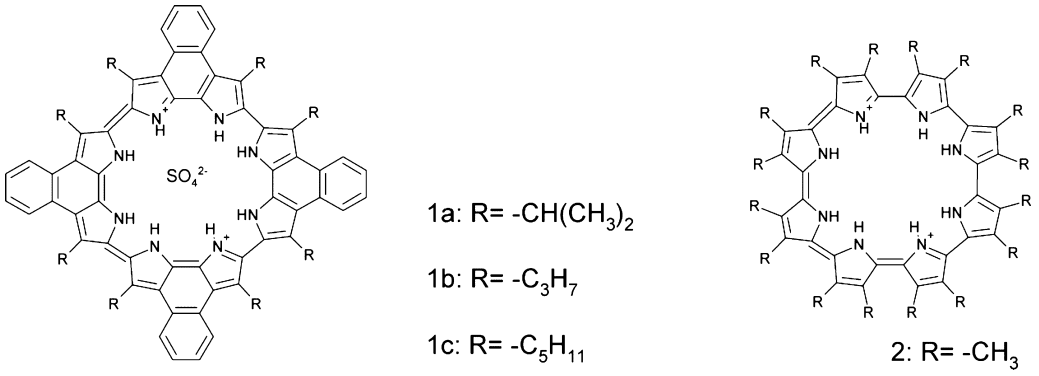

pair of InGaAs detectors were used for the UV/vis region and for the 800−1700 nm range, respectively. Spectral grade solvents were obtained from Merck (perchloric acid, dichloromethane, acetonitrile) and Roth (*N*,*N*-dimethylformamide). A saturated water solution of NaOH was prepared using distilled water (18.2 MΩ cm^{-1}, Millipore Direct-Q machine). All measurements were carried out at room temperature.

Raman measurements were performed using an InVia Renishaw system based on a Leica microscope and equipped with a thermoelectrically cooled 1024 × 256 CCD detector and 1800 l/mm grating. The 514.5 nm Ar^+ laser line (Stellar Pro argon Modu-Laser, LLC, 50 mW) was used as the excitation source. The spectra were collected by a ×100 objective (NA = 0.85, Leica) or by a 30 mm focal point (Renishaw) objective from crystalline and solution samples, respectively. To avoid decomposition of the crystalline sample, the power of the laser was decreased 100 times by gray filters and the measurement was carried out by raster scanning in the *XY* plane with a 2 μm step and 1 s integration time. The spectra of solutions in dichloromethane (Roth, spectroscopic grade) and acetonitrile (Merck, spectroscopic grade) were measured in 10 mm quartz cuvette. Series of spectra were registered for 12 h with the time window of 6 s. This was followed by averaging over 1000 spectra. In addition to providing a good signal-to-noise ratio, such a procedure allowed us to check for possible decomposition caused by prolonged irradiation. No such changes were detected in the Raman spectra during 12 h.

Geometry optimizations were performed using density functional theory (DFT), with the B3LYP functional and 6-31G(d,p) basis set, as implemented in the Gaussian 09 package.[58] The same functional and basis set were applied in the TD-DFT calculations of transition energies. Alternatively, the ZINDO model, based on a semiempirical INDO/S approximation[59] was used. The same INDO/S model was used in the DZDO program, which allowed calculating the MCD parameters. The DZDO program, originally developed by John Downing and Josef Michl, has been expanded to accommodate up to 200 sp atoms, up to 200 hydrogens, and up to 1000 electrons. The possible number of configurations in the configuration interaction (CI) procedure was 2000. Because the geometry of the molecules under investigation (and, as a consequence, excited state characteristics) are affected by the peripheral alkyl substituents, they had to be explicitly included into the calculations, which made them fairly time-consuming. Therefore, in some cases, optimizations using a semiempirical AM1 method were applied in the initial stage.

3. RESULTS AND DISCUSSION

3.1. Absorption and MCD Spectra. The electronic absorption and MCD spectra of **1a**−**1c** are presented in Figures 1−3. Table 1 compares the observed and calculated transition energies and MCD signs. This table contains DZDO computational results, as only this method is able to calculate MCD parameters. We also performed ZINDO calculations for **1a** using the X-ray geometry and TD-DFT calculations using

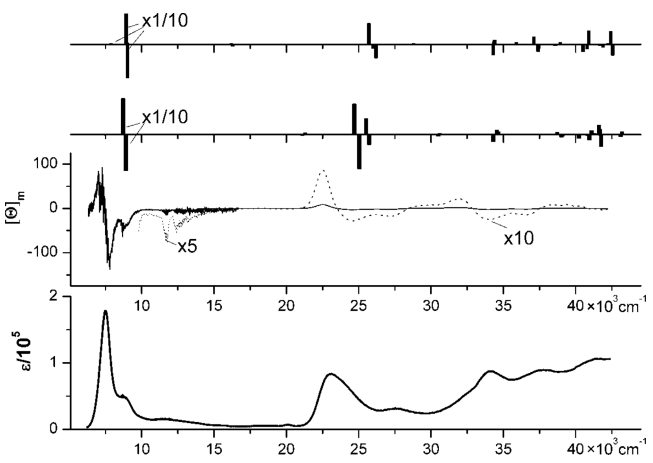

Figure 1. From bottom to top: absorption and MCD spectra of **1a**. MCD pattern calculated using DZDO for the X-ray geometry without and with the SO_4^{2-} anion included.

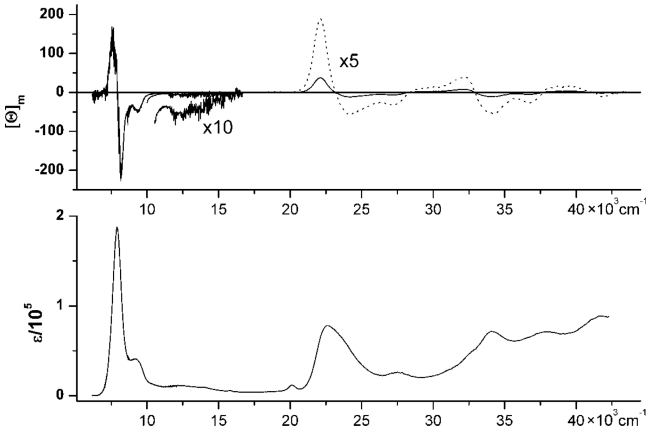

Figure 2. Absorption and MCD spectra of **1b**.

dx.doi.org/10.1021/jp412139r | J. Phys. Chem. A 2014, 118, 1038−1046

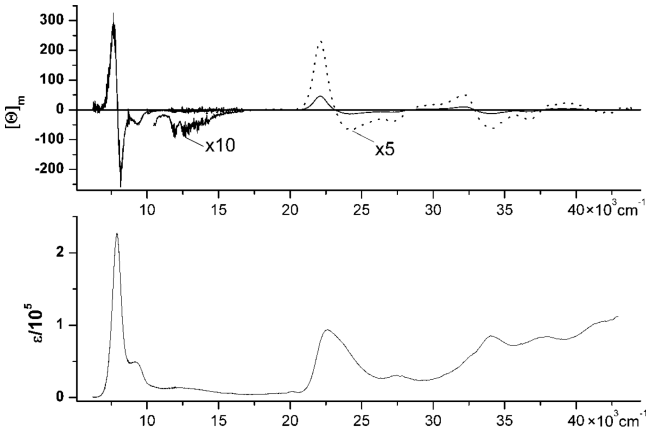

Figure 3. Absorption and MCD spectra of **1c**.

the geometry optimized with the same functional and basis set (B3LYP/6-31G(d,p)). All three methods gave very similar results. The agreement with experiment was excellent for the most intense transitions observed at 7500 and 22 600 cm^{-1}: the corresponding values were 7400/7600 and 22 600/23 000 (ZINDO), 8700/8900 and 24 700/25 000 (DZDO), and 9100/9100 and 25 300/25 300 cm^{-1} (TD-DFT). The values obtained by TD-DFT deviate from the experimental values somewhat more than those predicted by semiempirical models. On the other hand, TD-DFT was more accurate in reproducing the energies of weaker transitions. For instance, the band observed at 11 500 cm^{-1} was predicted by TD-DFT to lie at 10 900 cm^{-1}, whereas both DZDO and ZINDO overestimated its location, yielding 15 700 and 16 200 cm^{-1}, respectively.

The spectra of all three derivatives are very similar, but a distinct difference is revealed between **1a** and **1b**/**1c**: in the former the lowest energy band is red-shifted by 400 cm^{-1} with respect to the position observed for **1b** and **1c**. This suggests a slight difference in the structure of the isopropyl-substituted derivative, which may be due to steric interactions. A more detailed discussion of the problem of nonplanarity is presented below.

Both absorption and MCD spectra strongly resemble those of **2**[36] in the energy region below 30 000 cm^{-1}. Two strong band systems (L and B in Platt's terminology used for aromatic compounds[60]) are observed in the absorption: the lowest energy, highest intensity transition is red-shifted by 1200−1600 cm^{-1} in **1a**−**1c** compared to the position in **2**. In contrast, a strong, higher energy band is observed exactly at the same location, 22 600 cm^{-1} in **1a**−**1c** and in **2**. Also, the maximum absorption coefficients are very similar for this region, whereas they are about twice as high for **1a**−**1c** in comparison with **2** for the low-energy band. This effect was reproduced by calculations of oscillator strengths in doubly protonated **1a** and **2**.

At least three electronic transitions of weak intensity are detected between the L and B bands. For the region above 30 000 cm^{-1} both absorption and MCD indicate the presence of a large number of electronic states. This could be expected as a consequence of adding naphthalene units to the chromophoric system. The absorption and MCD reveal different intensity patterns, which allows detecting transitions overlapping in the absorption. A good example is provided by a transition around 34 500 cm^{-1}, observed as a shoulder in absorption, but clearly distinguished as a positive peak in the MCD curves of **1a**−**1c**.

Similarly to the case of **2**, **1a**−**1c** reveal a characteristic MCD pattern for L and B bands: a strong positive signal, followed by

Table 1. Observed and Calculated Electronic Transitions of 1a−1c

experiment[a]						calculations[b]			
1a		**1b**		**1c**		**1a**			
Abs[c]	MCD[c,d]	Abs	MCD	Abs	MCD	energy	f[e]	B term[f]	dominant configuration[g]
7.5	7.1 (−)	7.9	7.6(−)	7.9	7.6(−)	8.7	1.37	−8140	0.92(1,−1)
	7.8(+)		8.2(+)		8.1(+)	8.9	1.29	+8198	0.92(2,−1)
8.74	8.8(+)	9.2	9.4(+)	9.2	9.4(+)				
11.5	11.8(+)	12.1	12.0(+)	12.0	11.8(+)	15.7	0.01	−2	0.56(6,−1)
	12.4(+)				12.6(+)	15.7	0.01	+3	0.76(7,−1)
		13.9	13.7(+)						
15.9		15.9		15.9		16.3	0.03	+4	0.82(3,−1)
19.1		19.0		19.2		21.1	0.26	+21	0.89(8,−1)
						21.3	0.31	−43	0.92(9,−1)
22.6	22.5 (−)	22.6	22.1(−)	22.6	22.1(−)	24.7	3.82	−694	0.87(1,−2)
	24.6(+)		24.3(+)		24.2(+)	25.0	3.65	+774	0.85(2,−2)
27.4	27.3(+)	27.4	27.2(+)	27.4	27.2(+)	25.5	0.05	−367	0.67(1,−3) − 0.56(2,−4)
						25.7	0.32	+228	0.59(2,−3) + 0.59(2,−4)
	29.1(−)		29.0(−)		28.7(−)	29.4	0.15	−7	0.62(2,−4)
						30.9	0.13	+2	0.55(4,−2)
32.7sh	32.1(−)	32.4sh	32.4(−)	32.4sh	32.3(−)	34.3	0.60	+164	0.68(1,−6)
						34.5	0.38	−101	0.53(2,−6)
34.1	34.0(+)	34.1	34.1(+)	34.1	34.2(+)	34.7	0.29	−59	0.60(3,−2)
	36.6(+)		36.8(+)		36.9(+)	37.8	0.14	−11	0.43(7,−2)
37.7	38.3(−)	37.7		37.8	38.9(−)	38.7	0.17	−54	0.56(1,−10)
41.6	41.8(+)	41.6	41.7(+)	41.5	41.7(+)	39.0	0.19	+55	0.55(2,−10)

[a] CH_2Cl_2 solution, 293 K. [b] DZDO, X-ray geometry, 196 lowest singly excited configurations. [c] 10^3 cm^{-1}. [d] In parentheses, sign of the Faraday B term. [e] Oscillator strength. [f] $10^{-3}D^2\mu_B/cm^{-1}$, μ_B is the Bohr magneton. [g] The occupied orbitals are labeled 1, 2, ..., where HOMO=1, $(-n)$ denotes the nth lowest LUMO orbital.

dx.doi.org/10.1021/jp412139r | J. Phys. Chem. A 2014, 118, 1038−1046

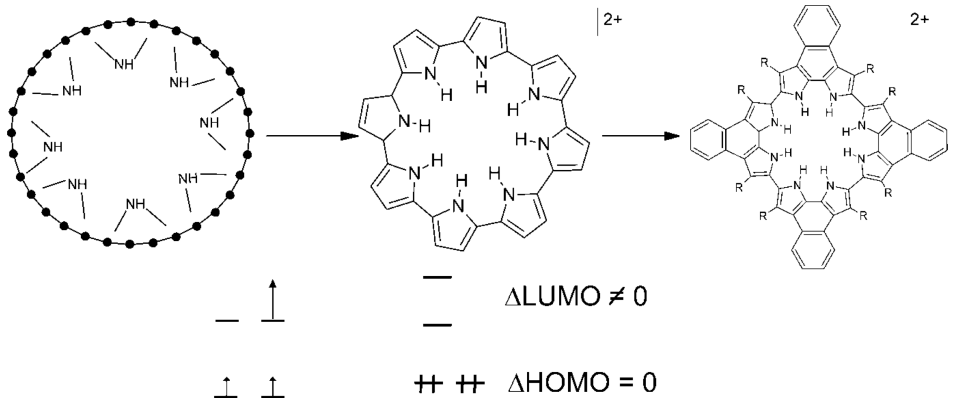

Figure 4. Formal derivation of cyclo[4]naphthobipyrroles from the $C_{32}H_{32}^{2+}$ perimeter, accompanied by lowering of degeneracy of the LUMO orbitals.

a negative one of similar intensity. Such a pattern can be interpreted either as a −,+ sequence of Faraday *B* terms corresponding to two close-lying electronic transitions, or to a negative Faraday *A* term due to a degenerate electronic state. The derivative shape of the MCD curve in the region of the lowest electronic transition, together with the observation that the MCD signal changes sign at the wavelength of absorption maximum, suggest a degeneracy or pseudodegeneracy, described by the Faraday *A* or pseudo-*A* term, expected for a structure with a high-symmetry axis. However, in the region of B bands such shape is not observed as clearly as it was in the case of **2**, cyclohepta-, and cyclohexapyrroles.[36] It is clear that a larger number of electronic transitions contribute to the spectra in this region.

3.2. Perimeter Model Analysis. The strong resemblance of the electronic spectra of **1a−1c** to those of **2** suggests to analyze cyclo[4]naphthobipyrroles in terms of a perimeter model, an approach that allows us to understand and predict patterns and trends in absorption and MCD spectra of $4N + 2$ π-electron chromophores.[54,61,62] The perimeter model has been successfully used in the analysis of electronic structure and spectra of numerous aromatic molecules,[63] including cyclohexa-, cyclohepta-, and cyclooctapyrroles.[36] We now extend it to **1a−1c**, treating them as derivatives of **2**.

Cyclooctapyrrole **2** may formally be derived from a regular $C_nH_n^{2+}$ annulene containing $(4N + 2)$ π electrons ($n = 32$, $N = 7$). The orbitals ψ_k and ψ_{-k} ($k = 0, 1, ...$) of an ideal perimeter are pairwise degenerate (except for $k = 0$ and $k = n/2$ if n is even). They may be envisaged as representing an electron circulating along the perimeter, in the opposite directions for ψ_k and ψ_{-k}. The four lowest excited states (observed as L and B transitions) are described in the perimeter model in a 2×2 basis of four frontier orbitals. For $C_{32}H_{32}^{2+}$ the pairs of highest occupied orbitals, HOMO, and of lowest unoccupied ones, LUMO, correspond to ψ_{15}, ψ_{-15} and ψ_{16}, ψ_{-16}, respectively. A symmetry-lowering perturbation can lift the orbital degeneracy for all or only certain pairs, depending on symmetry. Adding eight −NH- linkers to $C_{32}H_{32}^{2+}$ leads to doubly charged cyclooctapyrrole (Figure 4). The symmetry is lowered, but a rotation axis of high order still remains: C_8 if the molecule is planar or if all pyrrole units are tilted in the same direction, or C_4 if each pyrrole unit is tilted in the direction opposite to that of its nearest neighbors. For each of these two cases, symmetry considerations based on the properties of cyclic groups predict which pairs of orbitals are no longer degenerate. In $C_{32}H_{32}^{2+}$ it is the LUMO pair, whereas the degeneracy of two HOMO orbitals remains. Thus, $\Delta HOMO = 0 \ll \Delta LUMO$. Explicit expressions for the dipole strength, as well as for the signs and magnitudes of the Faraday *A* and *B* terms have been obtained for the L and B bands of an ideal perimeter.[54] A crucial quantity in these formulas is the difference in the absolute values of HOMO and LUMO splitting. If ΔHOMO and ΔLUMO are similar, the sign sequence of the Faraday terms can easily be changed by a symmetry-lowering perturbation, such as substitution, bridging, tautomerization, etc. However, this is not the case for $\Delta HOMO \neq \Delta LUMO$. Now, the perturbation is not expected to change the "inherent" pattern. These predictions have led to a nomenclature, according to which the chromophores sensitive to perturbations ($\Delta HOMO \approx \Delta LUMO$) are called "soft", whereas those which are not ($\Delta HOMO \neq \Delta LUMO$) are referred to as "hard". For cyclo[*n*]pyrroles, symmetry considerations lead to the expectation of $\Delta HOMO \ll \Delta LUMO$, which implies[54] that the *A* terms should be negative for both L and B transitions, whereas the *B* term should be positive for the L and negative for the B state. These predictions are in excellent agreement with experiment.[36]

Cyclo[4]naphthobipyrroles **1a−1c** can be derived from **2** (Figure 4) taking into account four different types of perturbations: (a) linking with four biphenylene units; (b) adding eight alkyl substituents; (c) binding a sulfate dianion in the central cavity; (d) possible distortion from planarity. These perturbations can lead to the loss of effective high-order symmetry; in such a case, the *A* terms should no longer be observed. We note, however, that as long as the two components of L and B transitions are close in energy, each *A* term evolves smoothly into a pair of *B* terms of opposite signs, and the general MCD pattern changes very little. Although the issue of exact or quasi-degeneracy is difficult to resolve, the MCD pattern observed for **1a−1c** leaves no doubt about the relative disposition of the frontier π orbitals. In an aromatic $4N + 2$ electron system, the −,+, −,+ sequence of *B* terms (or two negative *A* terms) indicates that the energy splitting between the two highest occupied orbitals is smaller than the splitting between the two lowest unoccupied ones: $\Delta HOMO \ll \Delta LUMO$. In a high-symmetry system, the HOMO orbitals should be exactly degenerate, but they no longer need to be so in **1a−1c**. In principle, one could analyze separately the influence of four different types of perturbation on the orbital energy shifts. Due to the complexity of the systems under study, a more practical approach is to check whether the calculations, which implicitly include all the

dx.doi.org/10.1021/jp412139r | J. Phys. Chem. A 2014, 118, 1038−1046

perturbational effects, predict the orbital sequence strongly suggested by the experiment. We consider this problem in the next section.

3.3. Geometrical and Electronic Structure of the Cyclo[4]naphthobipyrrole Chromophore. A reliable analysis of the electronic structure and spectra requires the knowledge of ground state geometry. Given the size of cyclo[4]naphthobipyrroles, geometry optimization is a challenging and computationally demanding task. Moreover, many local minima are to be expected due to various possible relative orientations of naphthobipyrrolic units, internal protons, and the alkyl substituents. We therefore adopted a different strategy of estimating the ground state geometry, based on the experimental, crystallographic, and spectral evidence. The X-ray structure of **1a** is known.[55,56] The macrocycle assumes a saddle conformation, but a considerable degree of planarity is retained (the angle between adjacent naphthobipyrrolic units is about 30°). This may be due to the stabilizing effect of the sulfate anion, which binds to the inner core via eight NH···O hydrogen bonds of similar lengths (193−199 pm).

The question now arises whether the spectra we record in solution correspond to the sulfate-containing species with the geometry resembling that obtained by X-ray analysis or to a dissociated species, for which a different structure can be expected. The answer was provided by comparing the Raman spectra obtained for crystalline samples with the spectra measured in solution. The results of such a comparison for **1b** are presented in Figure 5. The spectra obtained for the crystal are practically the same as those recorded in dichloromethane. Because of much poorer solubility in acetonitrile, the spectra are more noisy, but they also strongly resemble those measured for two other environments.

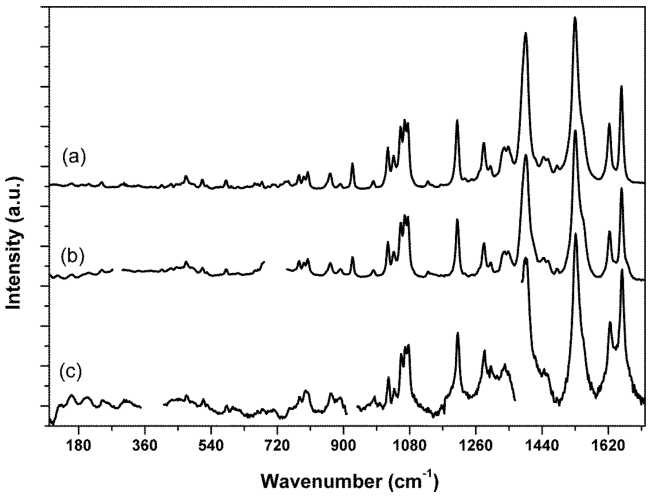

Figure 5. Raman spectra of **1b**: (a) crystalline phase; (b) dichloromethane; (c) acetonitrile. For (b) and (c) the solvent contribution has been subtracted; this is indicated by discontinuities in the spectral curves.

This behavior can readily be understood if the chromophore exists in solution as an uncharged, undissociated form. We conclude that the absorption and MCD spectra presented in Figures 1−3, as well as the Raman spectra in Figure 5, correspond to the species containing the sulfate ion in the cavity. This result is in line with poor solubility of **1a**−**1c** in polar solvents.

A strong support for such a conclusion is provided by calculations of the transition energies and intensities, performed while assuming the X-ray geometry of the chromophore. The transition energies, intensities, and the MCD patterns, calculated for **1a**, are in excellent agreement with experimental spectra (Table 1). Moreover, we have performed the calculations for two cases: (a) a complex with the SO_4^{2-} ion inside; (b) a structure with the same geometry, but without the SO_4^{2-} ion. Very similar results were obtained in both situations (Figure 1): for (a) the calculations predict a number of additional, low-intensity transitions, but the most intense ones, dominating the spectrum are changed very little with respect to those calculated for "bare" **1a**.

The calculations now allow us to check the predictions regarding the orbital energy disposition. Even though the symmetry is now lower, the orbital splitting is exactly as expected for a more symmetric chromophore: the HOMO orbitals are nearly degenerate, whereas a large splitting is obtained for the LUMO pair (ZINDO calculations yield ΔHOMO = 0.08 eV, ΔLUMO = 2.40 eV). Practically the same orbital splittings are predicted for the sulfate-containing form (ΔHOMO = 0.07 eV, ΔLUMO = 2.70 eV), confirming the lack of significant influence of the sulfate on the electronic structure of **1**. The frontier orbitals are presented in Figure 6. It is to be noted that they strongly resemble those of **2**, which explains the similarities between cyclo[4]naphthobipyrroles and cyclo[8]-pyrrole.

These results point to several important conclusions. First, the presence of the anion in the inner cavity induces spectral changes via modification of the geometry of the chromophore rather than by altering the electronic structure. Second, one can expect that the geometry of the chromophore is strongly sensitive to the presence of an anion in the inner cavity. Finally, modification of the geometry can result in large spectral changes, in particular in the region of the lowest energy band.

In principle, comparison of the transition energies of complexed, hydrogen-bonded species with those of the uncomplexed chromophore could give insight into the hydrogen bonding properties in different electronically excited states.[64] In view of the above conclusions, however, such a procedure would be rather risky, as the transition energy differences would contain a major contribution caused by geometry rearrangement, difficult to separate from that due to changes in hydrogen bonding strength. An estimation of the hydrogen bonding strength changes was done for the electronic states corresponding to the strongest electronic transitions observed around 7000−9000 and 22 600 cm^{-1} (Table 1). The transition energies of **1a**, calculated for the same chromophore geometry of the uncomplexed and complexed species, revealed a small red shift of about 200 cm^{-1} in the latter, indicating a very small increase of the hydrogen bond energy upon excitation (one should remember that this value corresponds to the contribution from eight bonds!).

The attempts to establish the geometry of a solvated dication, without the dianion in the cavity were not conclusive, because using different theoretical models did not converge to the same pattern. DFT geometry optimizations of the "bare" dication led to a saddle-type structure of approximately D_{2d} symmetry, similar to the structure of the complex known from X-ray measurements. The main difference was in the angles formed by naphthobipyrrole units, larger than in the uncomplexed dication by about 10° (40° vs 30°). The spectral patterns predicted for the complexed and uncomplexed species

dx.doi.org/10.1021/jp412139r | J. Phys. Chem. A 2014, 118, 1038−1046

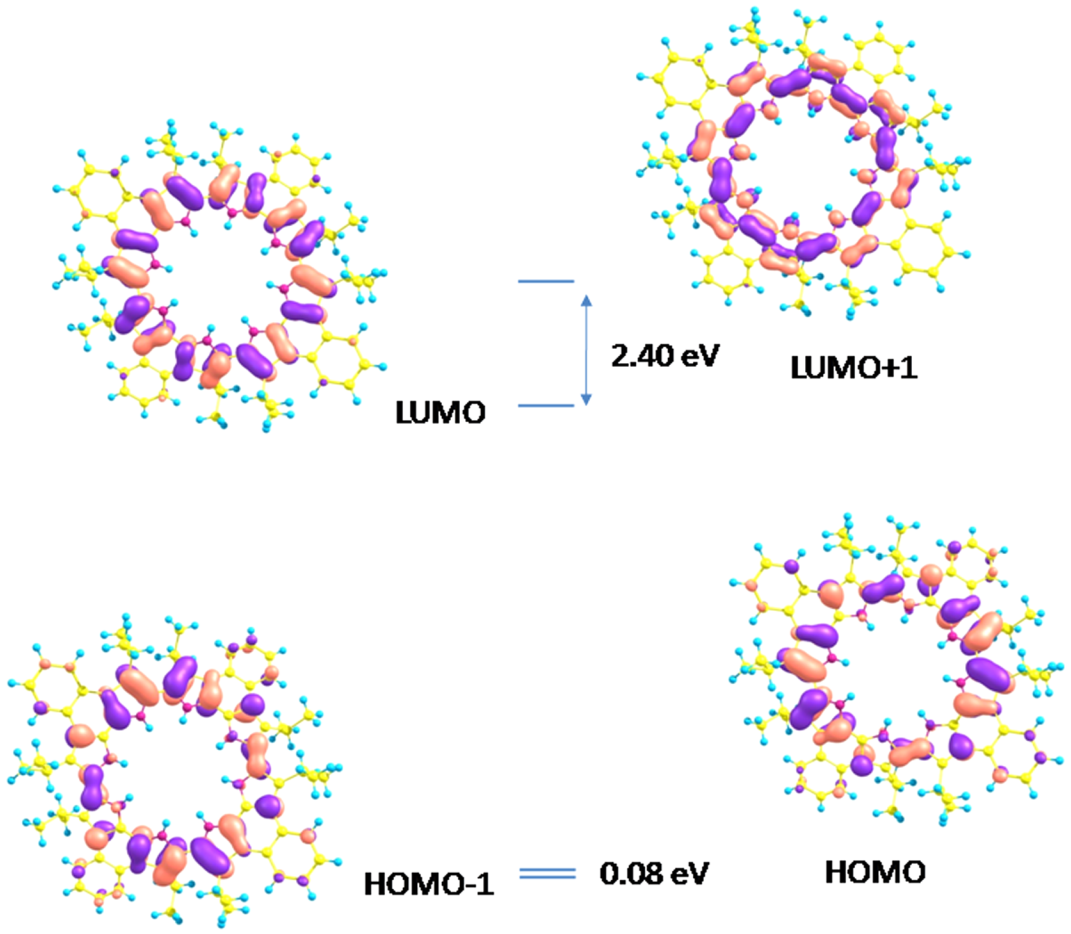

Figure 6. Frontier orbitals of **1a**, calculated using ZINDO for the X-ray geometry.

are similar and correspond nicely to the spectra recorded in solution. In turn, optimizations using AM1 resulted also in a saddle-like geometry, but now the ZINDO-calculated pattern of excited state energies and transition intensities was quite different. This result should, however, be taken with caution, as it is known that the methods based on Hartree−Fock approximations yield an unrealistic, distorted structure of tetrapyrroles.[65] One can also envisage a dome-like structure of the dication (all four units tilted in the same direction), stabilized by a specific interaction with a polar solvent. We tried to optimize the geometry starting from a dome-shaped species, but the calculations always converged into a saddle-like structure, with the neighboring naphthobipyrrole units tilted in opposite directions. It is possible that, to obtain a different geometry, the solvent molecule(s) should explicitly be taken into account. Moreover, to properly assess the role of the interactions between the naphthobipyrrole blocks and the solvent effects, one should eliminate the influence of alkyl substituents, by synthesizing the chromophore without eight alkyl units. Unfortunately, such structure is not available yet. However, we simulated the structure of diprotonated cyclo[4]-naphthobipyrrole not containing peripheral substitutents. The optimized geometry corresponds to a much more planar structure: the angles formed by naphthobipyrrole units are now about 2°. For **1a**, optimized using the same model, these angles are 37° (Figure 7), indicating that the nonplanarity of **1a**−**1c** is mainly caused by alkyl substitutents. The excited state patterns calculated using ZINDO for both geometries are quite similar, but the energies of both L and B transitions shift to the blue in the more planar form, by ca. 1600 and 2500 cm^{-1}, respectively.

Very interesting spectral changes were observed upon adding $HClO_4$ to a solution in dichloromethane neutralized by washing with aqueous NaOH solution (Figure 8). Now, the intensity of the strong transition observed around 1300 nm decreases, and new, weaker bands appear in the range between 700 and 1000 nm. Very similar spectral changes have been reported for **2** during its first controlled potential oxidation in CH_2Cl_2; the spectrum was therefore assigned to the radical cation.[46] We have observed similar behavior also for other mixtures: (i) CH_2Cl_2 + $HClO_4$ (without adding NaOH); (b) chloroform + trifluoroacetic acid; (c) methanol + H_2SO_4.

We also tried to obtain the spectra of neutral species. The spectral changes observed while bases were added to the solutions were quite complex, depending on solvent and a particular derivative. For instance, Figure 9 shows the absorption changes observed for the samples obtained upon washing toluene solutions of **1a** and **1c** with aqueous NaOH solution. For **1a**, a band growing around 1500 nm is observed, indicating a red shift upon deprotonation. Similar behavior was observed for DMSO solutions of all three compounds. On the other hand, **1c** reveals, in the same toluene/NaOH mixture, a completely different behavior. Now, the blue-shifted band is observed around 1080 nm. The same blue-shifted pattern is observed for **1a** when its CH_2Cl_2 solution is shaken with aqueous NaOH (Figure 7b). A spectacular decrease in absorption and MCD intensity is observed (Figure 10). The

dx.doi.org/10.1021/jp412139r | J. Phys. Chem. A 2014, 118, 1038−1046

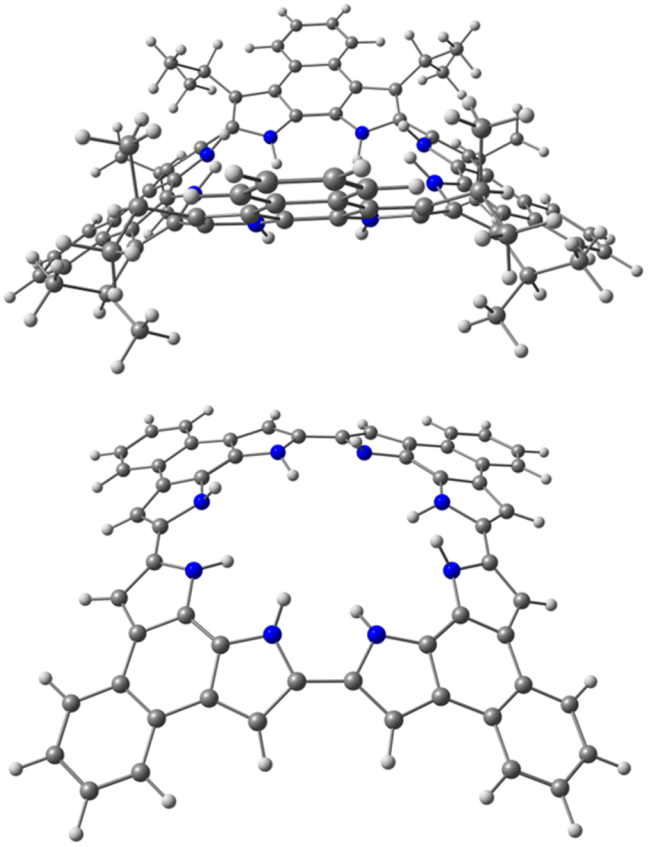

Figure 7. B3LYP/6-31G(d,p)-optimized ground state geometry of **1a** (top) and of the same chromophore not containing isopropyl substituents (bottom).

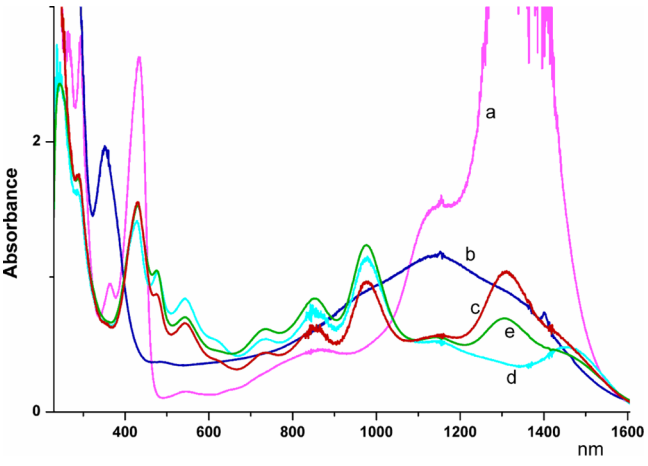

Figure 8. Absorption spectra of **1a**: (a) pure CH_2Cl_2; (b) after washing with water solution of NaOH; (c), (d) solution (b) after adding 24 and 32 droplets of $HClO_4$, respectively; (e) solution (d) measured after 48 h.

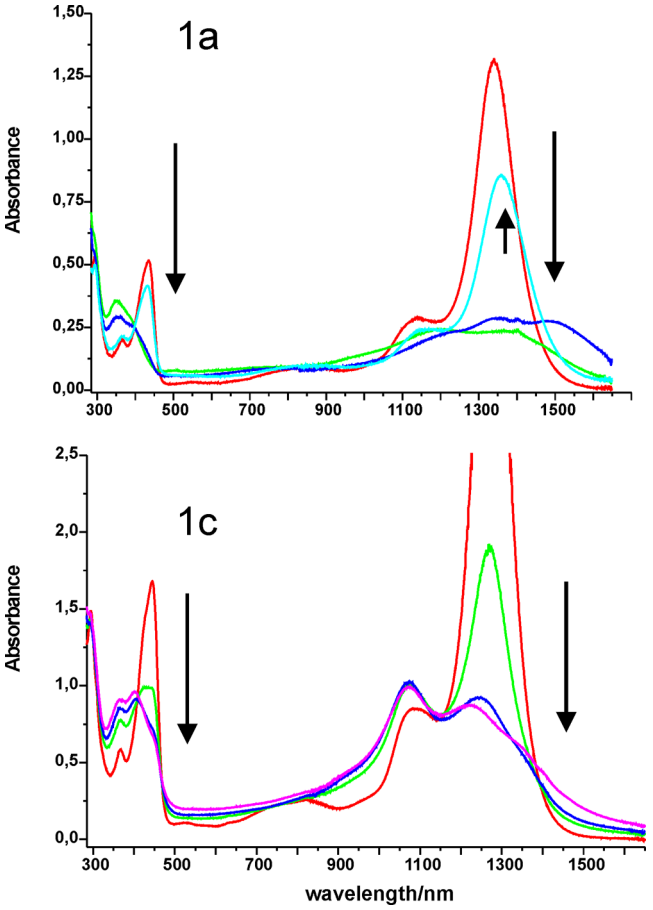

Figure 9. Changes in absorption of **1a** (top) and **1c** (bottom) in toluene upon addition of NaOH. The upward pointing arrow shows reprotonation observed upon adding H_3PO_4 to the solution containing the neutral form.

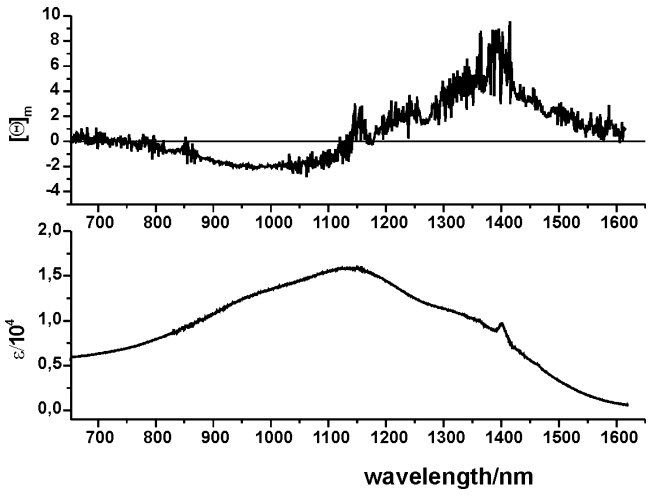

Figure 10. Absorption and MCD of **1a** in the low-energy region, measured in CH_2Cl_2/NaOH mixture.

low-energy band is now much broader and red-shifted, but the +,− MCD pattern (−,+ sequence of *B*) is preserved. This complicated behavior points to the existence of tautomeric equilibria, structure sensitivity, and solvent sensitivity. We optimized the geometry of various possible tautomeric forms of neutral **1a**; this was followed by DZDO calculations of absorption and MCD patterns. For two species, the theoretically obtained absorption predicted a red shift upon deprotonation. Both of them correspond to the two protons being removed from the opposite naphthobipyrrole units. For the tautomers with two nonprotonated nitrogen atoms residing on the same or neighboring blocks, the predicted spectral patterns were very different: in particular, a blue shift was predicted for the lowest energy band. Interestingly, the calculated ground state energies of the forms for which the

dx.doi.org/10.1021/jp412139r | J. Phys. Chem. A 2014, 118, 1038−1046

red shift was predicted, were calculated about 2 and 6 kcal/mol higher than that of the most stable form. We note, however, that the error in predicting relative tautomer stabilities may be quite large for molecules which have 492 normal modes, of which about 60 have frequencies comparable with or lower than kT (at 293 K). Again, it should be stressed that the calculations do not take into account the solvent effects.

4. SUMMARY

The electronic absorption spectra of three differently alkyl-substituted cyclo[4]naphthobipyrroles strongly resemble each other, as well as the spectra of hexadecamethylcyclo[8]pyrrole. This allows describing the electronic structure of **1a**−**1c** in terms of the perimeter model, treating these molecules as derivatives of **2**. The compounds belong to the so-called "negative-hard chromophores", characterized by the energy difference between the two lowest unoccupied LUMO orbitals being much larger than the energy difference between the HOMO pair. The $\Delta\mathrm{HOMO} \ll \Delta\mathrm{LUMO}$ inequality allows us to predict the relative intensities in absorption and MCD, as well as the pattern of MCD signs. The orbital energy splitting pattern in **1a**−**1c** is the same as in a high-symmetry chromophore.

The "negative-hard" character of cyclo[8]pyrroles has been recently confirmed by the studies of acenaphthylene-fused derivatives.[53] The reported absorption and MCD patterns were very similar to those of **1a**−**1c**.

Both experiment and theory strongly suggest that in solution, similarly to the crystalline phase, **1a**−**1c** exist in the form of complexes with the SO_4^{2-} dianion residing in the inner cavity. The calculations, as well as the initial experiments performed for basic solutions, suggest that the geometry of the chromophore and, as a consequence, the electronic spectra should be sensitive to several factors: the degree of protonation of the inner cavity, the nature of peripheral substituents, and possibly, the presence or absence of a complexed anion. Differentiating between complexed and noncomplexed species should be possible on the basis of electronic absorption and/or MCD. Two particular aspects of the spectroscopy of cyclo[4]-naphthobipyrroles are important in this context. First, the electronic transition expected to be most affected by anion release is the strongest one in the absorption. Second, the near-IR location of the corresponding band is unique and very rarely encountered in other chromophores. Therefore, cyclo[4]-naphthobipyrroles emerge as good models for studying molecular recognition phenomena, also in complex systems, such as biological membranes, because of the possibility to monitor the binding events in the range where the spectra are not perturbed by the presence of other chromophores. Still, one has to remember that, for analytical applications, the binding ability for a particular anion should not be too strong, because for such a case the equilibrium between the complexed and uncomplexed species will be dominated by the former. Exactly such a case seems to be occurring for the sulfate anion, of which the structure enables simultaneous forming of eight hydrogen bonds with cyclo[8]pyrroles.

AUTHOR INFORMATION

Notes

The authors declare no competing financial interest.

ACKNOWLEDGMENTS

This work has been financed by the funds from the Polish National Science Centre (DEC-2011/01/B/ST4/01130 and DEC-2011/02/A/ST5/00443) and Department of Science and Technology (DST), India (SR/S1/IC-56/2012 to P.K.P.). We acknowledge a computing grant from the Interdisciplinary Centre for Mathematical and Computational Modeling. This research was also supported in part by PL-Grid Infrastructure. T.S. thanks Council of Scientific and Industrial Research (CSIR), India, for the financial support.

REFERENCES

(1) Sessler, J. L.; Burrell, A. K. *Top. Curr. Chem.* **1992**, *161*, 177−273.
(2) Sessler, J. L.; Burrell, A. K.; Furuta, H.; Hemmi, G. W.; Iverson, B. L.; Král, V.; Magda, D. J.; Mody, T. D.; Shreder, K.; Smith, D.; Weghorn, S. J. *NATO ASI Ser., Ser. C* **1994**, *448*, 391−408.
(3) Sessler, J. L.; Weghorn, S. J. *Expanded, Contracted & Isomeric Porphyrins*; Elsevier: Oxford, U.K., 1997.
(4) Jasat, A.; Dolphin, D. *Chem. Rev.* **1997**, *97*, 2267−2340.
(5) Sessler, J. L.; Tvermoes, N. A.; Davis, J.; Anzenbacher, P., Jr.; Jursikov, K.; Sato, W.; Seidel, D.; Lynch, V.; Black, C. B.; Try, A.; Andrioletti, B.; Hemmi, G.; Mody, T. D.; Magda, D. J.; Kral, V. *Pure Appl. Chem.* **1999**, *71*, 2009−2018.
(6) Ravi, K. M.; Chandrashekar, T. K. *J. Inclusion Phenom. Macrocycl. Chem.* **1999**, *35*, 553−582.
(7) Sessler, J. L.; Gebauer, A.; Weghorn, S. J. In *The Porphyrin Handbook*; Kadish, K. M., Smith, K. M., Guilard, R., Eds.; Academic Press: New York, 2000; Vol. 2, pp 55−124.
(8) Sessler, J. L.; Camiolo, S.; Gale, P. A. *Coord. Chem. Rev.* **2003**, *240*, 17−55.
(9) Sessler, J. L.; Seidel, D. *Angew. Chem., Int. Ed.* **2003**, *42*, 5134−5175.
(10) Chandrashekar, T. K.; Venkatraman, S. *Acc. Chem. Res.* **2003**, *36*, 676−691.
(11) Shimizu, S.; Osuka, A. *J. Porphyrins Phthalocyanines* **2004**, *8*, 175−181.
(12) Král, V.; Králová, J.; Kaplánek, R.; Bříza, T.; Martásek, P. *Physiol. Res.* **2006**, *55* (Suppl 2), S3−26.
(13) Sessler, J. L.; Tomat, E. *Acc. Chem. Res.* **2007**, *40*, 371−379.
(14) Jux, N. *Angew. Chem., Int. Ed.* **2008**, *47*, 2543−2546.
(15) Misra, R.; Chandrashekar, T. K. *Acc. Chem. Res.* **2008**, *41*, 265−279.
(16) Yoon, Z. S.; Osuka, A.; Kim, D. *Nat. Chem.* **2009**, *1*, 113−122.
(17) Shin, J.-Y.; Kim, K. S.; Yoon, M.-C.; Lim, J. M.; Yoon, Z. S.; Osuka, A.; Kim, D. *Chem. Soc. Rev.* **2010**, *39*, 2751−2767.
(18) Anzenbacher, P., Jr. *Top. Heterocycl. Chem.* **2010**, *24*, 237−265.
(19) Osuka, A.; Saito, S. *Chem. Commun. (Cambridge, U. K.)* **2011**, *47*, 4330−4339.
(20) Saito, S.; Osuka, A. *Angew. Chem., Int. Ed.* **2011**, *50*, 4342−4373.
(21) Stępień, M.; Sprutta, N.; Latos-Grażyński, L. *Angew. Chem., Int. Ed.* **2011**, *50*, 4288−4340 S4288/4281−S4288/4282..
(22) Arambula, J. F.; Preihs, C.; Borthwick, D.; Magda, D.; Sessler, J. L. *Anti-Cancer Agents Med. Chem.* **2011**, *11*, 222−232.
(23) Pareek, Y.; Ravikanth, M.; Chandrashekar, T. K. *Acc. Chem. Res.* **2012**, *45*, 1801−1816.
(24) Le, G. S.; Boitrel, B. *J. Porphyrins Phthalocyanines* **2012**, *16*, 537−544.
(25) Sessler, J. L.; Karnas, E.; Sedenberg, E. *Supramolecular Chemistry: From Molecules to Nanomaterials*; John Wiley & Sons Ltd.: New York, 2012; Vol. 3, pp 1045−1073.
(26) Gale, P. A.; Haynes, C. J. E. *Supramolecular Chemistry: From Molecules to Nanomaterials*; John Wiley & Sons Ltd.: New York, 2012; Vol. 3, pp 1125−1151.
(27) Calvete, M. J. F. *Int. Rev. Phys. Chem.* **2012**, *31*, 319−366.
(28) Mody, T. D.; Sessler, J. L. *J. Porphyrins Phthalocyanines* **2001**, *5*, 134−142.

(29) Pushpan, S. K.; Venkatraman, S.; Anand, V. G.; Sankar, J.; Parmeswaran, D.; Ganesan, S.; Chandrashekar, T. K. *Curr. Med. Chem.: Anti-Cancer Agents* **2002**, *2*, 187−207.
(30) Ortiz de Montellano, P. R.; Evans, J. P.; Serradell, N.; Bolos, J.; Rosa, E. *Drugs Future* **2007**, *32*, 601−606.
(31) Sessler, J. L.; Gebauer, A.; Vogel, E. In *The Porphyrin Handbook*; Kadish, K. M., Smith, K. M., Guilard, R., Eds.; Academic Press: New York, 2000; Vol. *2*, pp 1−54.
(32) Shimizu, S.; Aratani, N.; Osuka, A. *Chem.—Eur. J.* **2006**, *12*, 4909−4918.
(33) Yoon, M.-C.; Kim, P.; Yoo, H.; Shimizu, S.; Koide, T.; Tokuji, S.; Saito, S.; Osuka, A.; Kim, D. *J. Phys. Chem. B* **2011**, *115*, 14928−14937.
(34) Seidel, D.; Lynch, V.; Sessler, J. L. *Angew. Chem., Int. Ed.* **2002**, *41*, 1422−1425.
(35) Köhler, T.; Seidel, D.; Lynch, V.; Arp, F. O.; Ou, Z.; Kadish, K. M.; Sessler, J. L. *J. Am. Chem. Soc.* **2003**, *125*, 6872−6873.
(36) Gorski, A.; Köhler, T.; Seidel, D.; Lee, J. T.; Orzanowska, G.; Sessler, J. L.; Waluk, J. *Chem.—Eur. J.* **2005**, *11*, 4179−4184.
(37) Köhler, T.; Ou, Z.; Lee, J. T.; Seidel, D.; Lynch, V.; Kadish, K. M.; Sessler, J. L. *Angew. Chem., Int. Ed.* **2005**, *44*, 83−87.
(38) Xu, H.; Yu, G.; Xu, W.; Xu, Y.; Cui, G.; Zhang, D.; Liu, Y.; Zhu, D. *Langmuir* **2005**, *21*, 5391−5395.
(39) Baker, E. S.; Lee, J. T.; Sessler, J. L.; Bowers, M. T. *J. Am. Chem. Soc.* **2006**, *128*, 2641−2648.
(40) Bucher, C.; Devillers, C. H.; Moutet, J.-C.; Pecaut, J.; Sessler, J. L. *Chem. Commun. (Cambridge, U. K.)* **2006**, 3891−3893.
(41) Sessler, J. L.; Lee, J. T.; Ou, Z.; Köhler, T.; Hargrove, A. E.; Cho, W.-S.; Lynch, V.; Kadish, K. M. *J. Porphyrins Phthalocyanines* **2006**, *10*, 1329−1336.
(42) Yoon, Z. S.; Kwon, J. H.; Yoon, M.-C.; Koh, M. K.; Noh, S. B.; Sessler, J. L.; Lee, J. T.; Seidel, D.; Aguilar, A.; Shimizu, S.; Suzuki, M.; Osuka, A.; Kim, D. *J. Am. Chem. Soc.* **2006**, *128*, 14128−14134.
(43) Eller, L. R.; Stępień, M.; Fowler, C. J.; Lee, J. T.; Sessler, J. L.; Moyer, B. A. *J. Am. Chem. Soc.* **2007**, *129*, 11020−11021.
(44) Melfi, P. J.; Kim, S. K.; Lee, J. T.; Bolze, F.; Seidel, D.; Lynch, V. M.; Veauthier, J. M.; Gaunt, A. J.; Neu, M. P.; Ou, Z.; Kadish, K. M.; Fukuzumi, S.; Ohkubo, K.; Sessler, J. L. *Inorg. Chem.* **2007**, *46*, 5143−5145.
(45) Stępień, M.; Donnio, B.; Sessler, J. L. *Angew. Chem., Int. Ed.* **2007**, *46*, 1431−1435.
(46) Sessler, J. L.; Karnas, E.; Kim, S. K.; Ou, Z.; Zhang, M.; Kadish, K. M.; Ohkubo, K.; Fukuzumi, S. *J. Am. Chem. Soc.* **2008**, *130*, 15256−15257.
(47) Alkorta, I.; Blanco, F.; Elguero, J. *Cent. Eur. J. Chem.* **2009**, *7*, 683−689.
(48) Buda, M.; Iordache, A.; Bucher, C.; Moutet, J.-C.; Royal, G.; Saint-Aman, E.; Sessler, J. L. *Chem.—Eur. J.* **2010**, *16*, 6810−6819.
(49) Karnas, E.; Kim, S. K.; Johnson, K. A.; Sessler, J. L.; Ohkubo, K.; Fukuzumi, S. *J. Am. Chem. Soc.* **2010**, *132*, 16617−16622.
(50) Lee, J. T.; Chae, D.-H.; Ou, Z.; Kadish, K. M.; Yao, Z.; Sessler, J. L. *J. Am. Chem. Soc.* **2011**, *133*, 19547−19552.
(51) Bui, T.-T.; Iordache, A.; Chen, Z.; Roznyatovskiy, V. V.; Saint-Aman, E.; Lim, J. M.; Lee, B. S.; Ghosh, S.; Moutet, J.-C.; Sessler, J. L.; Kim, D.; Bucher, C. *Chem.—Eur. J.* **2012**, *18*, 5853−5859 S5853/5851−S5853/5818..
(52) Bui, T.-T.; Escande, A.; Philouze, C.; Cioci, G.; Ghosh, S.; Saint-Aman, E.; Lim, J. M.; Moutet, J.-C.; Sessler, J. L.; Kim, D.; Bucher, C. *J. Porphyrins Phthalocyanines* **2013**, *17*, 27−35.
(53) Okujima, T.; Ando, C.; Mack, J.; Mori, S.; Hisaki, I.; Nakae, T.; Yamada, H.; Ohara, K.; Kobayashi, N.; Uno, H. *Chem.—Eur. J.* **2013**, *19*, 13970−13978.
(54) Michl, J. *J. Am. Chem. Soc.* **1978**, *100*, 6801−6811.
(55) Sarma, T.; Panda, P. K. *Chem.—Eur. J.* **2011**, *17*, 13987−13991 S13987/13981−S13987/13922.
(56) Roznyatovskiy, V. V.; Lim, J.-M.; Lynch, V. M.; Lee, B.-S.; Kim, D.-H.; Sessler, J. L. *Org. Lett.* **2011**, *13*, 5620−5623.
(57) (a) Anusha, P. T.; Swain, D.; Sarma, T.; Panda, P. K.; Venugopal, R. S. *Proc. SPIE* **2012**, *8434*, 84341D/84341−84341D/84346. (b) Swain, D.; Anusha, P. T.; Sarma, T.; Panda, P. K.; Venugopal, R. S. *Chem. Phys. Lett.* **2013**, *580*, 73−77.
(58) Frisch, M. J.; Trucks, G. W.; Schlegel, H. B.; Scuseria, G. E.; Robb, M. A.; et al. *Gaussian 09*, Revision B.01; Gaussian, Inc.: Wallingford, CT, 2010.
(59) Ridley, J. E.; Zerner, M. Z. *Theor. Chim. Acta* **1973**, *32*, 111.
(60) Platt, J. R. *J. Chem. Phys.* **1949**, *17*, 484−495.
(61) Michl, J. *J. Am. Chem. Soc.* **1978**, *100*, 6812−6818.
(62) Michl, J. *J. Am. Chem. Soc.* **1978**, *100*, 6819−6824.
(63) Michl, J. *Tetrahedron* **1984**, *40*, 3845−3934.
(64) Zhao, G. J.; Han, K. L. *Acc. Chem. Res.* **2012**, *45*, 404−413.
(65) Almlof, J.; Fischer, T. H.; Gassman, P. G.; Ghosh, A.; Haeser, M. *J. Phys. Chem.* **1993**, *97*, 10964−10970.